Seismic-Hazard Assessment for a Characteristic Earthquake Scenario: An Integrated Probabilistic–Deterministic Method

by Vincenzo Convertito,* Antonio Emolo, and Aldo Zollo

Abstract Probabilistic seismic hazard analysis (PSHA) is classically performed through the Cornell approach by using a uniform earthquake distribution over the source area and a given magnitude range. This study aims at extending the PSHA approach to the case of a characteristic earthquake scenario associated with an active fault. The approach integrates PSHA with a high-frequency deterministic technique for the prediction of peak and spectral ground motion parameters in a characteristic earthquake. The method is based on the site-dependent evaluation of the probability of exceedance for the chosen strong-motion parameter. The latter is obtained from the statistical analysis of the synthetic waveform database produced for a large number of possible rupture histories occurring on the characteristic earthquake fault. The method has been applied to a hazard evaluation in the Umbria region, where the threat is represented by a fault having the same geometry and mechanism as the 26 September 1997, Colfiorito earthquake (central Italy; moment magnitude, M_w 6).

Introduction

Since its formulation in 1968, probabilistic seismic hazard analysis (PSHA) (Cornell, 1968) has been one of the most widely used tools to evaluate the threat of seismic events in earthquake-prone zones. In particular, it finds large applications in regions where information about seismogenic structures is poor or not available for the application of deterministic seismic-hazard analyses.

The product of a PSHA is a hazard curve for a specified site representing the values of a selected strong ground motion parameter having a fixed probability of exceedance in a specified period. Each value takes into account the integrated effect of all the earthquakes of different sizes occurring in different seismic source zones (i.e., points, lines, areas, volumes, and faults) with different probabilities of occurrence.

One of the main steps in PSHA consists of evaluating the effects of an earthquake occurring at a given distance from a site of interest, and it is represented by the amplitude reached by the selected strong ground motion parameter (e.g., peak ground acceleration, velocity, or displacement or a spectral parameter) (Reiter, 1990). In general, this goal is pursued by using an attenuation relationship that is, in general an empirical relationship among parameters characterizing the source, the propagation medium, and the local site geology.

When a single causative fault and an associated maximum earthquake is considered as the threat for the site of interest, the application of the classical PSHA is not obvious. One problem is represented by the formulation of a recurrence relationship and the computation of the activity rate, in particular, for large-magnitude earthquakes for which the catalogs are generally not complete. Moreover, because of their empirical nature, the attenuation relationships provide ground-motion estimates and related uncertainties that account only partially for the characteristics of the earthquake source process and seismic wave propagation (Boore *et al.*, 1997; Somerville *et al.*, 1997; Convertito and Herrero, 2004). These features are of main concern for those sites located at distances comparable to the fault dimension insofar as the effect of source heterogeneity and complexity could be responsible for the complexity of ground motion high frequency ($f > 1$ Hz) records.

In contrast, the use of a purely deterministic approach for simulating the effect of a seismic event occurring on a given causative fault does not account for earthquake recurrence, thus providing a sort of "static" scenario that is of little use for probabilistic hazard evaluations. In this article, we propose a new integrated probabilistic–deterministic method aimed at overcoming some of the limitations of both PSHA and deterministic techniques when applied to a single fault (or fault system) for a scenario-like description of the hazard. In particular, it allows the time variable to be accounted for (i.e., in terms of return period and time of interest) in the deterministic scenario studies and for source pa-

*Present address: Istituto Nazionale di Geofisica e Vulcanologia, Osservatorio Vesuviano, 80124 Napoli, Italy.

rameters (geometry, radiation pattern, directivity, etc.) in the PSHA approach.

We use the "characteristic-earthquake" model to compute the probability of occurrence of earthquakes (Schwartz and Coppersmith, 1984) and the approach proposed by Youngs and Coppersmith (1985) to compute the activity rate. The characteristic-earthquake model is based on the observation that during repeated rupture episodes occurring on the same fault (or fault system), some characteristics, like fault geometry, source mechanism, and seismic moment, remain approximately constant over a large timescale; these parameters depend on the direction and intensity of the regional stress field. Relevant to the estimation of earthquake effects, the distance and azimuthal distribution of ground-motion parameters and their expected ranges of variability are obtained by applying the hybrid deterministic–stochastic method proposed by Zollo *et al.* (1997). The ground-motion estimates are validated by a comparison with empirical attenuation relationships. The technique developed in this article is applied to the case of the mainshock of the Umbria-Marche (central Italy) seismic sequence (Colfiorito earthquake, 26 September 1997, 09:40 UTC, M_w 6).

Theory Framework

The computation of a hazard curve requires the resolution of the classical hazard integral (Cornell, 1968), the formulation of which, for a selected strong ground motion parameter A and for the ith seismic source zone, is given by:

$$E_i(A \geq A_0) = \alpha_i \iint_{R\,M} f_R(r)\, f_M(m)\, p_a\, [A(m,r) \geq A_0 | m,\mathrm{r}]\, dm\, dr. \quad (1)$$

The quantity $E_i(A \geq A_0)$ in equation (1) represents the frequency of exceedance of a given threshold value A_0. If a Poissonian model for the earthquakes occurrence is assumed and a time of interest t is selected, the probability of exceedance $P(A \geq A_0, t)$ can be computed as:

$$P(A \geq A_0, t) = 1 - e^{-E_i(A \geq A_0)t}. \quad (2)$$

Once the geometry of the source and a range of magnitude of interest have been fixed, the probability density functions (PDFs) in equation (1) can be defined. In particular, $f_R(r)dr$ represents the probability of occurrence of a given earthquake at a distance in the range $(r, r + dr)$ from the site of interest. In general, this PDF has no analytical formulation except for some simple source geometries as a point or a line. The PDF $f_M(m)$ describes the probability of occurrence of each earthquake having a magnitude in a given range of interest. It can be easily shown that the latter PDF is a truncated exponential function when the Gutenberg–Richter recurrence relationship is used to characterize the occurrence of the earthquakes (Cornell and Van Marcke, 1969). The exceedance probability p_a represents the probability of exceedance of a threshold value A_0, for a given distance r and a given magnitude m. It depends on the ground-motion attenuation relationship and is, in general, computed assuming a lognormal distribution of the parameter A. Finally, the coefficient α_i represents the average rate of occurrence of the earthquakes for each zone, and it is usually estimated from seismic catalogs.

When a single causative fault is considered and the occurrence of a given magnitude earthquake is considered for a scenario-like analysis, equation (1) needs some modifications. In fact, it is not obvious what is the best formulation for the PDFs $f_R(r)$ and $f_M(m)$ and how to compute the parameter α_i. For the definition of distance, the best choice in the case of a single fault could be the minimum horizontal distance to the surface projection of the fault plane (e.g., Joyner and Boore, 1981), if one considers that the fault geometry and extension is known and that the rupture process involves the whole fault area, whatever the location of the nucleation point. In this case, the PDF $f_R(r)$ of the distance reduces to $1/dr$. The characteristic-earthquake model is a reasonable assumption for computing $f_M(m)$ for a large-magnitude event on a given fault (Schwartz and Coppersmith, 1984). This model is based on the hypothesis that individual faults tend to generate similar size or "characteristic" earthquakes and that characteristic earthquakes occur on a fault not at the exclusion of all other magnitudes, but with a frequency distribution different from an exponential one.

The observational basis of this model relies on both geological and seismological data. In fact, paleoseismic evidence in several different tectonic environments (e.g., Pantosti and Valensise, 1990; Pantosti *et al.*, 1993; Megharoui *et al.*, 2000) supports the idea that the rupture parameters of the earthquake (e.g., geometry, mechanism, and average slip per event) can be considered constant over a large timescale, with these parameters being mainly related to the regional stress regime. However, the details of the rupture process (e.g., nucleation and rupture propagation) need not remain identical in all events on the selected fault, as shown for example, by numerical simulation studies of fracture development (e.g., Rice, 1993; Nielsen *et al.*, 1995; Cochard and Madariaga, 1996). These processes are related to the variable rock strength and/or to the local stress conditions in the fault zone.

If the characteristic earthquake model is assumed, it is possible to formulate the corresponding $f_M(m)$ and to compute the activity rate following the approach proposed by Youngs and Coppersmith (1985). In particular, it can be demonstrated that the PDF $f_M(m)$ has the following expression:

$$f_M(m) = \begin{cases} 0 & \text{for } m < m_0 \\ \dfrac{\beta e^{-\beta(m-m_0)}}{1-e^{-\beta(m_{\max}-m_0-\Delta m_2)}} \dfrac{1}{1+C} & \text{for } m_0 \le m \le m_c = m_{\max} - \Delta m_2 \\ \dfrac{\beta e^{-\beta(m_{\max}-m_0-\Delta m_1-\Delta m_2)}}{1-e^{-\beta(m_{\max}-m_0-\Delta m_2)}} \dfrac{1}{1+C} & \text{for } m_c = m_{\max} - \Delta m_2 \le m \le m_{\max} \\ 0 & \text{for } m > m_{\max} \end{cases} \quad (3)$$

where the constant C is given by:

$$C = \frac{\beta e^{-(m_{\max}-m_0-\Delta m_1-\Delta m_2)}}{1 - e^{[-\beta(m_{\max}-m_0-\Delta m_2)]}} \Delta m_2; \quad (4)$$

with $\beta = b \ln 10$ (b is the b-value of the Gutenberg–Richter law), and $m_{\max}$ and m_0 are the maximum and minimum magnitude of interest, respectively. The parameters Δm_1 and Δm_2 represent two intervals, respectively, below and above the magnitude level m_c that is considered as the characteristic earthquake magnitude (Fig. 1). The values used by Youngs and Coppersmith (1985) in their applications for these two intervals are $\Delta m_1 = 1.0$ and $\Delta m_2 = 0.5$. Note that the characteristic behavior of $f_M(m)$ refers to earthquakes having a magnitude in the range $[m_c, m_{\max}]$ (the flat part in Fig. 1), and thus the same probability of occurrence. On the other hand, equation (3) for $m < m_c$ accounts for the noncharacteristic part of the PDF $f_M(m)$. Starting from equation (3), Youngs and Coppersmith (1985) showed that the seismic activity rate α_C for the characteristic part of the PDF $f_M(m)$ is given by:

$$\alpha_C = \alpha_{NC} \frac{\beta \Delta m_2 \, e^{-\beta(m_{\max}-m_0-\Delta m_1-\Delta m_2)}}{1 - e^{-\beta(m_{\max}-m_0-\Delta m_2)}}, \quad (5)$$

where

$$\alpha_{NC} = \frac{\mu A_f \tilde{S}[1 - e^{-\beta(m_{\max}-m_0-\Delta m_2)}]}{K M_0^{\max} e^{-\beta(m_{\max}-m_0-\Delta m_2)}} \quad (6)$$

represents the seismic-activity rate for the noncharacteristic part of the PDF $f_M(m)$. In equation (6), μ is the shear modulus, A_f is the total area of the considered fault plane, $\tilde{S}$ is the average slip rate along the fault, and $M_0^{\max}$ is the seismic moment evaluated for the maximum magnitude $m_{\max}$ by a relationship of the type $\log M_0 = cm + d$, relating the magnitude m to the seismic moment M_0 (e.g., Hanks and Kanamori [1979] law). The constant K is given by:

$$K = \frac{b10^{-c\Delta m_2}}{c - b} + \frac{be^{\beta \Delta m_1}(1 - 10^{-c\Delta m_2})}{c}. \quad (7)$$

Youngs and Coppersmith (1985) also determined an expression for the activity rate in the case of the exponential model for earthquakes occurrence, given by:

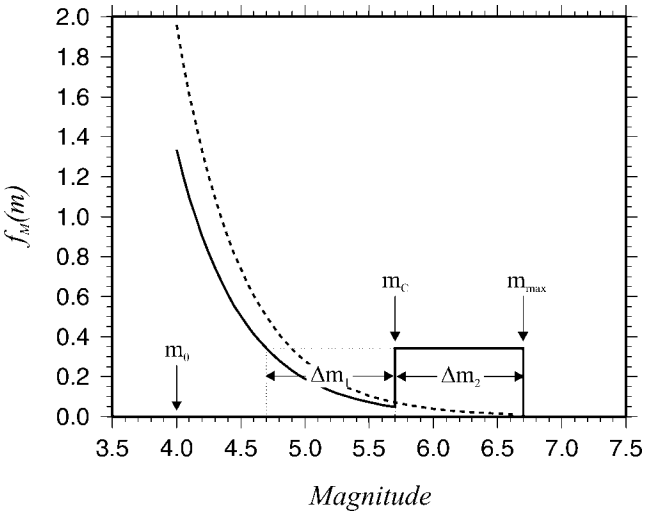

Figure 1. Magnitude PDF for the characteristic earthquake-recurrence model (black line) and for the truncated exponential earthquake-recurrence model (dashed line). See the text for the explanation of the parameters.

$$\alpha_{\exp} = \frac{\mu A_f \tilde{S}(c - b)[1 - e^{-\beta(m_{\max}-m_0)}]}{b M_0^{\max} e^{-\beta(m_{\max}-m_0)}}, \quad (8)$$

where the parameters are the same as in previous equations.

On the basis of the previous considerations, the classical hazard integral reported in equation (1) can be finally reformulated for the characteristic-earthquake model as follows:

$$E_i(A \ge A_0) = \alpha_C \int_{m_c}^{m_c+\Delta m_2} f_M(m) p_a[A(m,\bar{r}) \ge A_0 | m, \bar{r}] dm, \quad (9)$$

where $\bar{r}$, for each site of interest, represents the minimum distance from the surface projection of the ith rupturing fault, and α_c is given by equation (5). Thus, it is possible to compute the hazard curve for the single causative fault once the magnitude m_c for the characteristic earthquake has been selected. Of course, we also need a formulation for evaluating the level reached by the strong ground motion parameter A (i.e., the earthquake effect) and the associated exceedance probability p_a.

The Simulation of Ground Motion

To estimate the earthquake effects, we have adopted the method proposed by Zollo *et al.* (1997) that computes the ground motion associated with the rupture of a given fault solving the source representation integral (Aki and Richards, 1980). Details about the ground-motion simulation technique can be found in the Appendix.

A family of synthetic acceleration records was obtained by simulating a large number of rupture scenarios for a given fault plane. In the following section the application to the 1997 Umbria-Marche mainshock, where 150 different rupture scenarios are simulated, is discussed. Each rupture scenario has a different rupture nucleation point and final slip distribution. Heterogeneous slip on the fault is computed according to the *k*-square model of Hanks (1982) and Herrero and Bernard (1994). Each computed slip distribution is such that the total seismic moment corresponds to that of the considered characteristic earthquake. Rupture nucleation points were uniformly distributed in the deepest part of the fault, according to hypocentral determinations of the main events of the Umbria-Marche sequence (Zollo *et al.*, 1999). The maximum number of rupture scenarios to be simulated was chosen after having verified that no substantial differences in the estimation of mean values and standard deviations of the selected ground-motion parameter were observed for each receiver, by considering a larger number of simulations. For each rupture scenario we computed synthetic accelerograms on a regular grid of 64 receivers located in an area of about 60×60 km^2 (Fig. 2). The spacing between adjacent receivers was 5 km and the maximum frequency content of simulated accelerograms was 20 Hz.

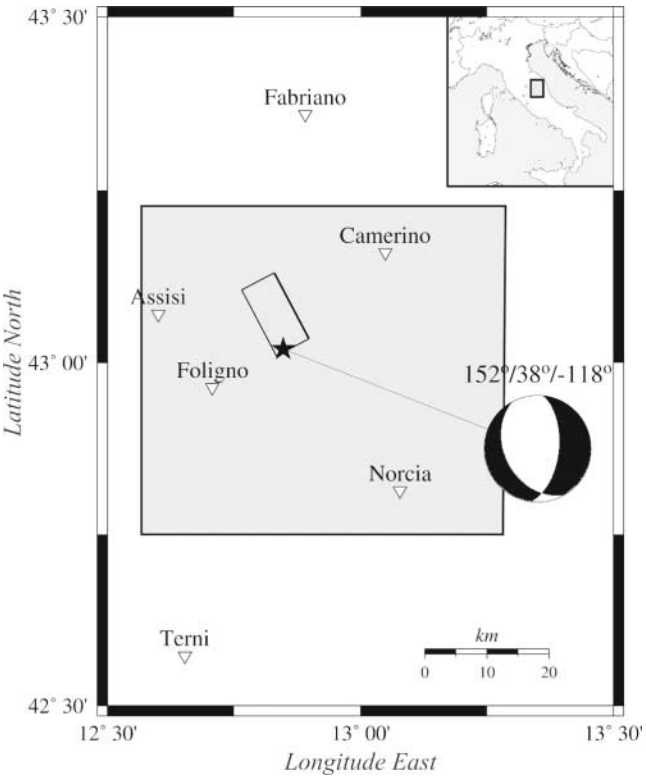

Figure 2. Epicentral area of the 1997 M_w 6 Colfiorito earthquake. The inner rectangle represents the surface fault projection and the star is the earthquake epicenter. The outer rectangle corresponds to the area considered in this study. The fault-plane solution after Zollo *et al.* (1999) and Capuano *et al.* (2000) is also shown.

Application and Results

The method proposed in this article has been applied to the 1997 M_w 6 Colfiorito mainshock of the Umbria-Marche sequence. The fault parameters used for the waveform simulation were determined by Zollo *et al.* (1999) and Capuano *et al.* (2000), and they are listed in Table 1.

Table 1
Fault Parameters Relative to the Mainshock of the Umbria-Marche (Central Italy) Seismic Sequence (Colfiorito Earthquake, 26 September 1997, 09:40 UTC, M_w 6) after Zollo *et al.* (1999) and Capuano *et al.* (2000)

Fault length	12 km
Fault width	7.5 km
Bottom depth	8 km
Strike	152°
Dip	38° (~SW)
Slip	−118°
Seismic moment	1.0×10^{18} N m
Rupture velocity	2.7 km/sec

The peak ground acceleration (PGA) is the selected ground-motion parameter for hazard analysis. The large number of simulated seismograms allowed a histogram to be built for each receiver, representing the frequency distribution of the PGA values. Through a chi-square test, we verified that the families of PGAs simulated at each receiver were lognormally distributed and could be characterized by a mean value with the associated statistical coefficient of variation [CoV = 100 (standard deviation/mean value)]. Thus, for each site, the probability of exceedance, p_a, in equation (9) could be finally computed by using the mean PGA value and the related uncertainty.

In Figure 3, the PGA and CoV maps are shown. The map of mean PGA values (Fig. 3a) shows a northwest–southeast alignment and a lobular trend associated with the source radiation pattern. This distribution can be compared with similar patterns observed in macroseismic maps (Tosi *et al.*, 1999). The largest predicted ground acceleration values (>2.0 m/sec^2) are observed north and southeast of the fault. We stress that the interpretation of the average map has to be carried out jointly with the CoV map. This map (Fig. 3b) shows the lowest values in the eastern region as a consequence of the up-dip source directivity. Regions where the CoV is higher (e.g., the western side of the map) indicate that the PGA values can vary strongly, depending on how

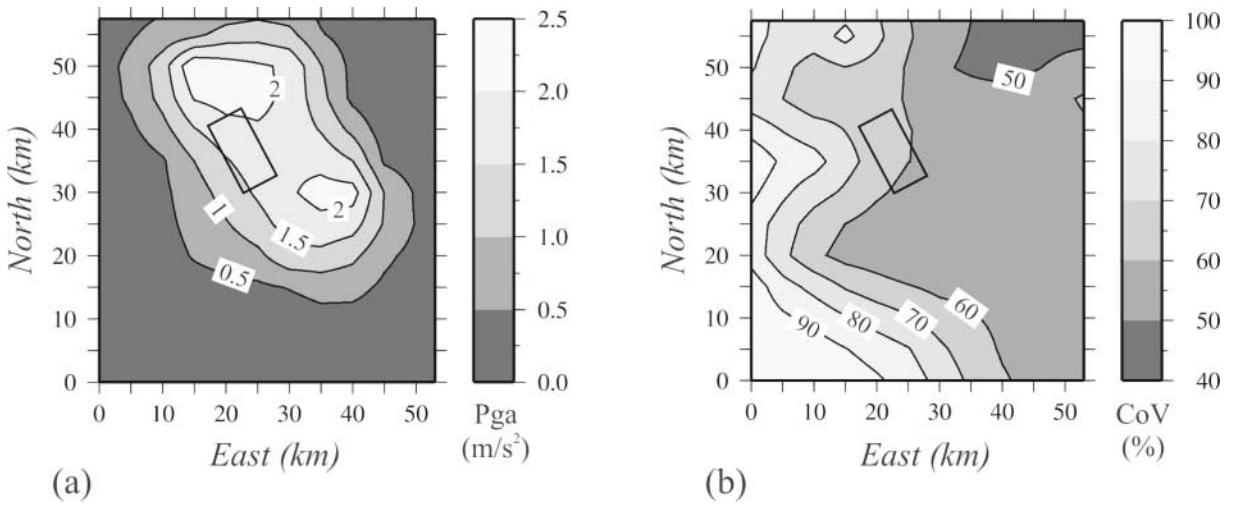

Figure 3. (a) Map of simulated PGA (mean values from 150 simulations). (b) Map of CoV (see the text for its definition). The rectangles in both figures represent the surface fault projection.

the rupture nucleates, propagates, and stops during the faulting process.

Synthetic PGA values as a function of the distance and the azimuth are given in Figure 4. The PGA variability along different profiles is controlled by fault geometry, directivity, and mechanism. Profiles located on the foot wall are characterized by PGA values larger than those for symmetrical profiles located on the hanging wall. This feature can be explained again as a dominant effect of the up-dip rupture directivity along with a geometrical source-to-receiver effect. This is not true for profiles 1 and 5. Indeed, the PGA attenuation along these profiles is clearly different. This behavior could be associated with a dominant effect of the source radiation pattern. In Figure 4, synthetic PGA ranges (plus/minus one standard deviation) are compared with the empirical attenuation curves proposed by Sabetta and Pugliese (1987) and Abrahamson and Silva (1997) for the M 6 event. In each panel, black continuous lines represent the Sabetta and Pugliese (1987) attenuation curve and gray lines the Abrahamson and Silva (1997) attenuation curves. In particular, continuous gray lines refer to sites located on the foot wall, and dashed gray lines refer to sites located on the hanging wall.

For a more complete comparison, the simulated and estimated PGA values for all of the profiles and for the two attenuation relationships are also given in Figure 4. We used the attenuation relationship proposed by Sabetta and Pugliese (1987) because it was derived from an Italian strong-motion database. We also selected the attenuation relationship proposed by Abrahamson and Silva (1997), insofar as it allows us to account for hanging- and foot-wall effects.

It is possible to distinguish profile directions in Figure 4 (e.g., profiles 5 and 8) for which the Sabetta and Pugliese (1987) attenuation relationship underestimates the predicted PGA values for distances larger than a few kilometers. In the same cases, the Abrahamson and Silva (1997) attenuation relationship provides PGA estimates at large distances that are similar to the simulated ones. On the other side, there are also profiles (e.g., profiles 2, 3, and 4) for which synthetic results are underestimated with respect to the empirical curves. Again, this is mainly due to the dominant up-dip rupture directivity in our synthetics.

The seismic activity rate for the characteristic part of the magnitude PDF (equation 5) is the final parameter needed to be computed to evaluate the hazard integral (equation 9). We retrieved the values of the parameters $b = 0.847$, $m_0 = 4.0$, and $m_{\max} = 6.7$ from the NT4.1 catalog (Camassi and Stucchi, 1996), values that characterize the seismic source zone in which the selected fault is embedded. Moreover, we adopted a slip rate $\tilde{S} = 0.385$ mm/year, which is the average value estimated for the seismogenic faults located in the Italian Apennines region (Valensise *et al.*, 2001). Finally, from the NT4.1 catalog, we estimated that the magnitude for which the characteristic behavior of the fault can be hypothesized ranges from M 5.7 to M 6.7. As a consequence, in our application we can select $\Delta m_1 = \Delta m_2 = 1.0$ in equations (3 4 5 6 7) and (9). With these assumptions, and using the fault parameters reported in Table 1, we obtained $\alpha_C = 0.000260$ years^{-1} from equation (5). Once the PGA, the associated CoV (Fig. 3), and the seismic-activity rate have been obtained, the hazard maps can be computed by using equation (9). The selected return periods for our analysis were $T_1 = 10{,}000$ years, $T_2 = 20{,}000$ years, and $T_3 = 50{,}000$ years.

For comparison with the classical Cornell (1968) approach we also performed the analysis for the truncated exponential model. Using equation (8), we computed the seismic activity rate for the same magnitude range ($M \in [5.7, 6.7]$), obtaining $\alpha_{\exp} = 0.0109$ years^{-1}. The hazard integral was then solved for the same geometry and magnitude range

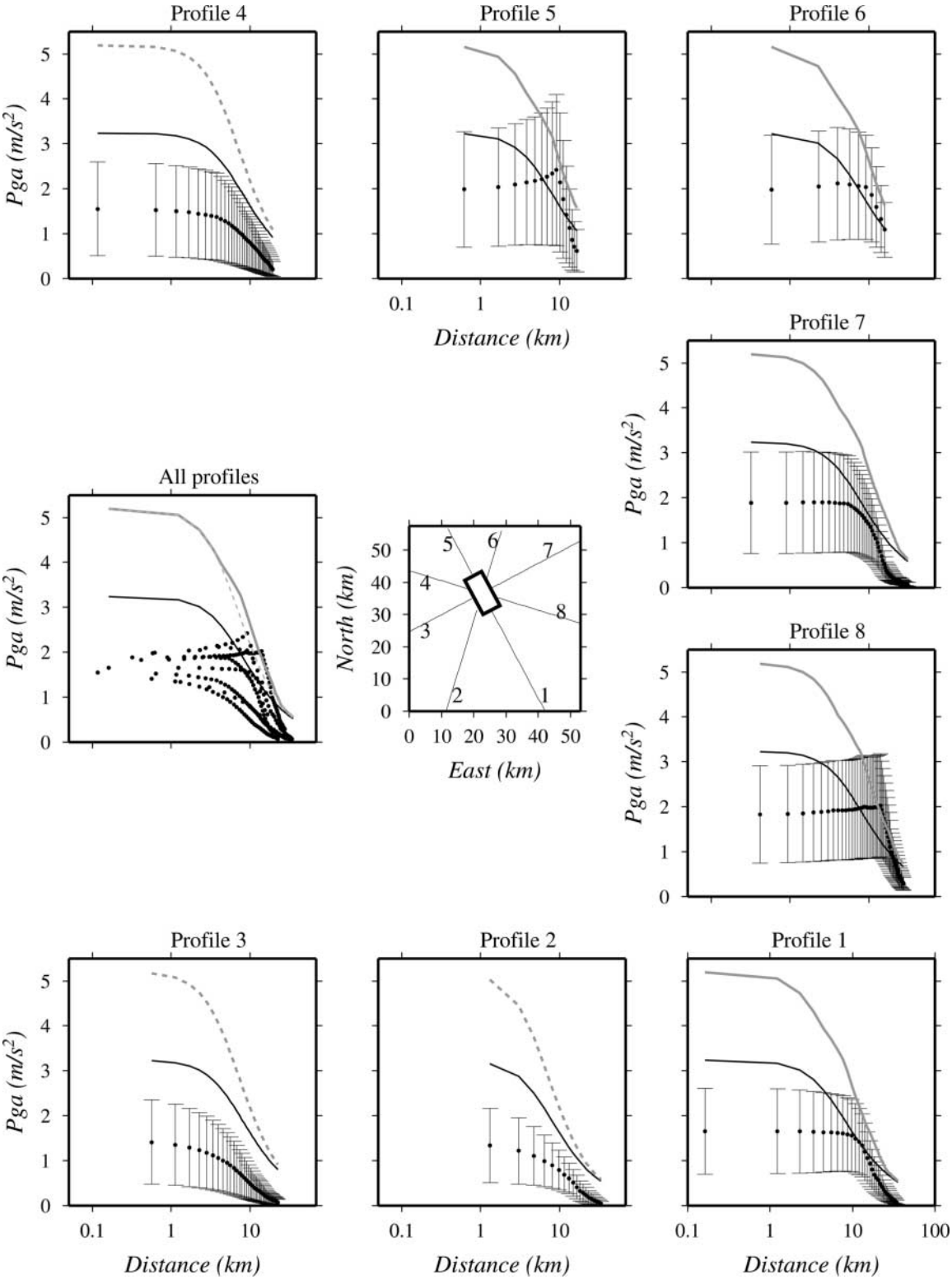

Figure 4. Plots of simulated PGA (mean values, black dots, plus/minus one standard deviation) versus the closest distance from the surface fault projection along different profiles around the fault. Profile 1 coincides with the fault-strike direction. The figures also report the Sabetta and Pugliese (1987) (black line) and Abrahamson and Silva (1997) (gray lines) relations for a M_w 6.0 earthquake. In particular, dashed gray lines refer to sites located on the hanging wall, and continuous gray lines refer to sites located on the foot wall. The mean PGA values for all profiles along with the estimate PGA values are also shown in the same figure.

and for both characteristic and exponential recurrence models, using two different attenuation relationships, Sabetta and Pugliese (1987) and Abrahamson and Silva (1997), for computing the probability of exceedance, p_a.

The results of the analysis for the return period $T_1 = 10{,}000$ years are reported in Figure 5, and those for periods $T_2 = 20{,}000$ years and $T_3 = 50{,}000$ years are shown in Figures 6 and 7, respectively. In each of Figures 5, 6, and 7, the top panels refer to the characteristic model and simulated PGAs (method presented in this article). Panels b and c show the results obtained for the characteristic model when the PGAs are estimated by using the Sabetta and Pugliese (1987) and Abrahamson and Silva (1997) attenuation relationships, respectively, whereas panels d and e correspond to the exponential models for the same attenuation relationships.

The hazard maps obtained from the synthetic data (panels a in Figs. 5, 6, and 7) reproduce the main features of the PGA map (Fig. 3a), thus accounting for kinematic seismic source parameters, such as the focal mechanism, the radiation pattern, and the directivity effect. This characteristic is more evident at larger return periods (panels a in Figs. 6 and 7).

In addition, we selected four sites located at the same distances from the surface fault projection to examine the differences between the results in the classical approach and in our method in site-specific hazard analysis. In particular, because of the fault geometry and orientation, site S1 is located on the foot wall, site S2 is located on the hanging wall, whereas sites S3 and S4 are off the end of the fault (Fig. 8). We computed the hazard curves for a 50-year exposure period (Figs. 9 and 10). As expected, for all four selected sites, there are no differences in the hazard curves when the PSHA with the Sabetta and Pugliese (1987) relation is applied, because of the symmetry of the problem. On the other hand, different results were obtained when an attenuation relationship that is able to account for the location or the azimuth of the site with respect to the orientation of the fault was used (the Abrahamson and Silva [1997] relation in our case). This is confirmed by the results shown in Figure 9 for sites 1 and 2 and in Figure 10 for sites 3 and 4.

The differences in the shapes of the hazard curves depend on the seismic-activity rates between the characteristic and the exponential recurrence models, the PGA estimates by the two different attenuation relationships with respect to the simulated values, and the differences among the standard deviations. In fact, although the two attenuation relationships are characterized by a constant value of the standard deviation, the synthetic results are characterized by a standard deviation that depends on the receiver position. Because this parameter controls the width and the long-tail shape of the lognormal distribution, the probability of exceedance in equation (9) retrieved from this distribution can be very different, depending on the site location (panels a of Figs. 9 and 10). In particular, for a given PGA value, the larger the distribution the larger is the probability of exceedance and the larger are the PGA threshold values (A_0 in equation 9) for which this probability can be evaluated. On the other hand, the differences in the hazard curves for sites S1 and S2 when the Abrahamson and Silva (1997) relation is used (Fig. 9e and i) are ascribed to the differences in the PGA estimates, depending on the site location relative to the fault mechanisms (i.e., hanging wall versus foot wall). In fact, when the sites are located on the same side or off the end of the faults, no difference is present in the hazard curves (Fig. 10e and i).

Discussion and Conclusions

In this article, we have proposed an original method that combines the probabilistic and the deterministic approaches in the hazard analysis. This technique is designed to overcome some of the limitations inherent in the deterministic and Cornell (1968) classical approaches when a single causative fault is considered for a scenario-like hazard analysis. In particular, we can account for the recurrence of a characteristic earthquake in the framework of the deterministic approach. In addition, the proposed method explicitly allows the incorporation of seismic source parameters in the PSHA, such as the radiation pattern, the fault geometry, and the directivity effect. Thus, some of the parameters that may affect the radiated energy in the near-source range and that cannot be easily considered by classical attenuation relationships can be accounted for.

Because of the availability of synthetic waveforms, the analyses performed in this article for PGA can be extended to any other ground-motion parameter, both in the time and frequency domains. Moreover, the site effect can be taken into account if the transfer functions are available.

We have shown the application of this method to the 1997 M_w 6 Colfiorito earthquake. We followed the approach proposed by Youngs and Coppersmith (1985) to compute the seismic-activity rates for both exponential and characteristic earthquake-recurrence models. The concept of a characteristic earthquake is then introduced in the formulation of the classical hazard integral (equation 1) by using a specific formulation of the magnitude PDF (equation 3). The PGA values obtained by the hybrid deterministic–stochastic simulation method (Zollo *et al.*, 1997) used in this application were first compared with estimates of the Sabetta and Pugliese (1987) and Abrahamson and Silva (1997) attenuation relationships (Fig. 4). The comparison illustrates that the simulated PGAs are comparable to the empirical estimates. An azimuthal dependence of synthetic data is evident, however.

We computed the hazard maps for three different return periods, $T_1 = 10{,}000$ years, $T_2 = 20{,}000$ years, and $T_3 = 50{,}000$ years, and we evaluated the hazard curves for four selected sites at a 50-year exposure period. The PGA distribution we retrieved (Figs. 5a, 6a, and 7a) can be ascribed to the way that the earthquake effects are accounted for in our technique. In particular, it is easy to recognize the source radiation pattern and directivity effects on our hazard maps. For each return period, the hazard maps obtained using syn-

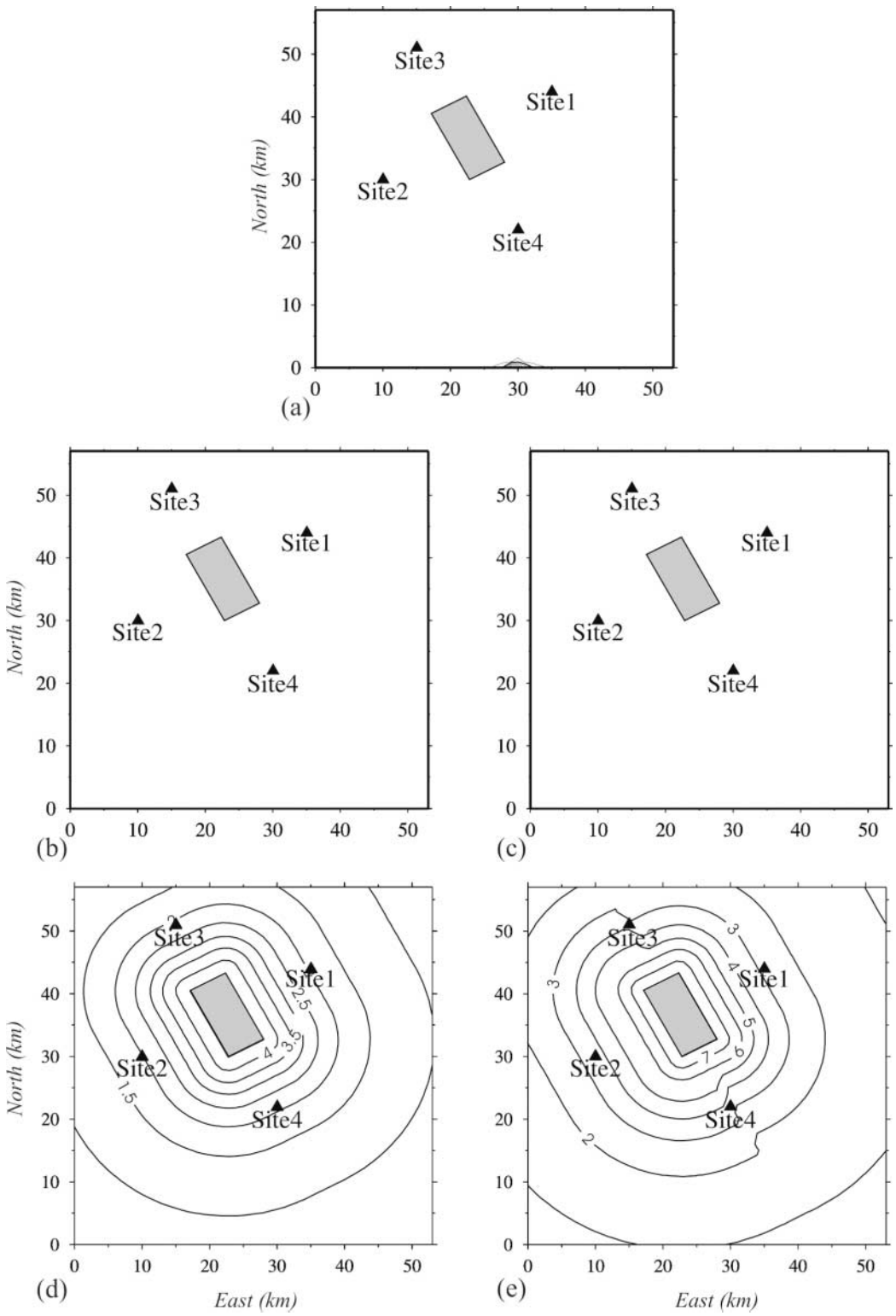

Figure 5. Hazard maps showing contours of PGA values having $T_1 = 10{,}000$ years return period and larger than 1 m/s^2. The gray box in each panel represents the surface fault projection. (a) Results for the characteristic model and simulated PGA values. (b) Hazard map for the characteristic model when the Sabetta and Pugliese (1987) attenuation relationship is used to estimate the PGA. (c) Hazard map for the characteristic model when the Abrahamson and Silva (1997) attenuation relationship is used to estimate the PGA. (d) Hazard map for the exponential model when the Sabetta and Pugliese (1987) attenuation relationship is used to estimate the PGA. (e) Hazard map for the exponential model when the Abrahamson and Silva (1997) attenuation relationship is used to estimate the PGA.

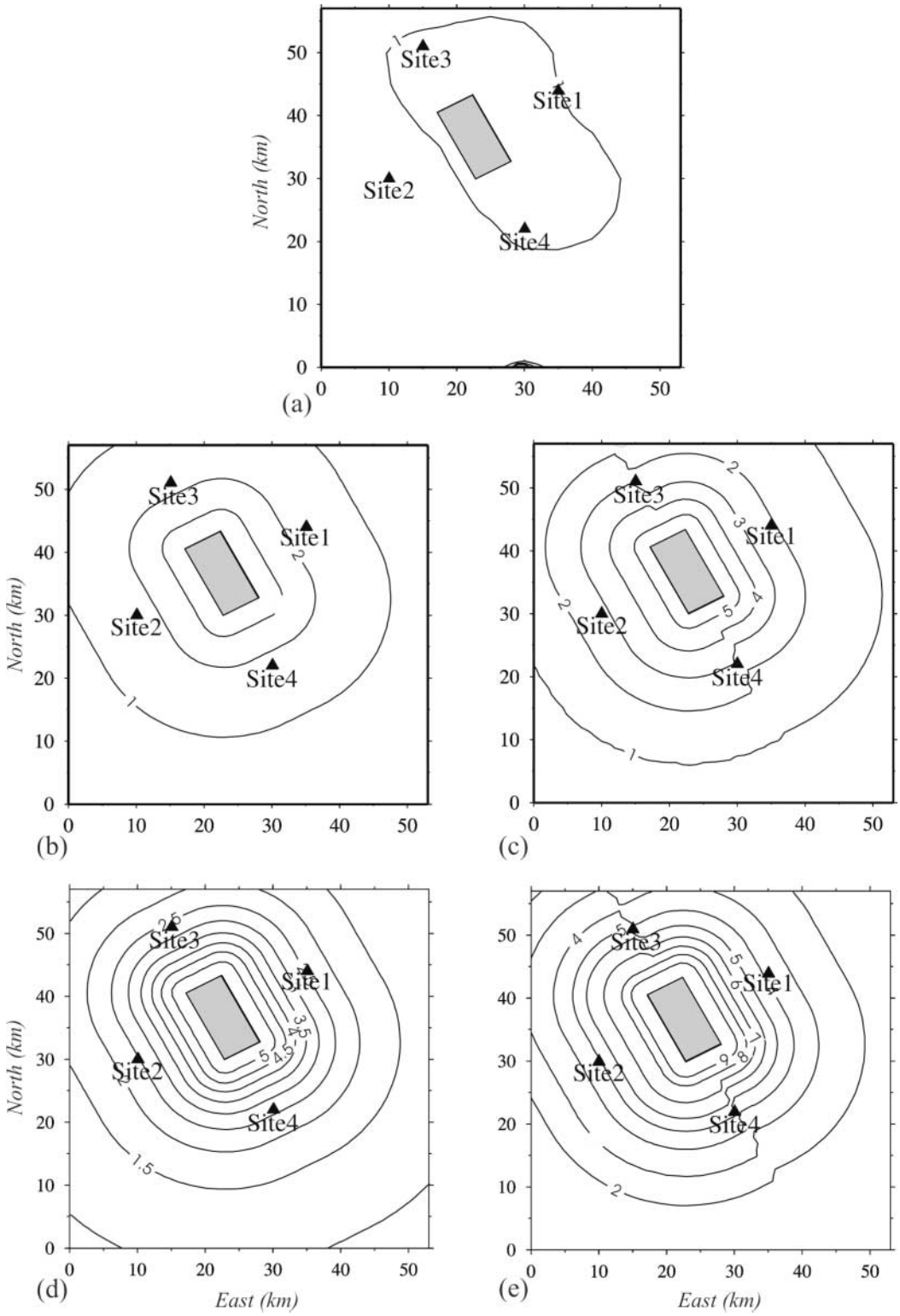

Figure 6. Same as Figure 5 but for $T_2 = 20{,}000$ years return period.

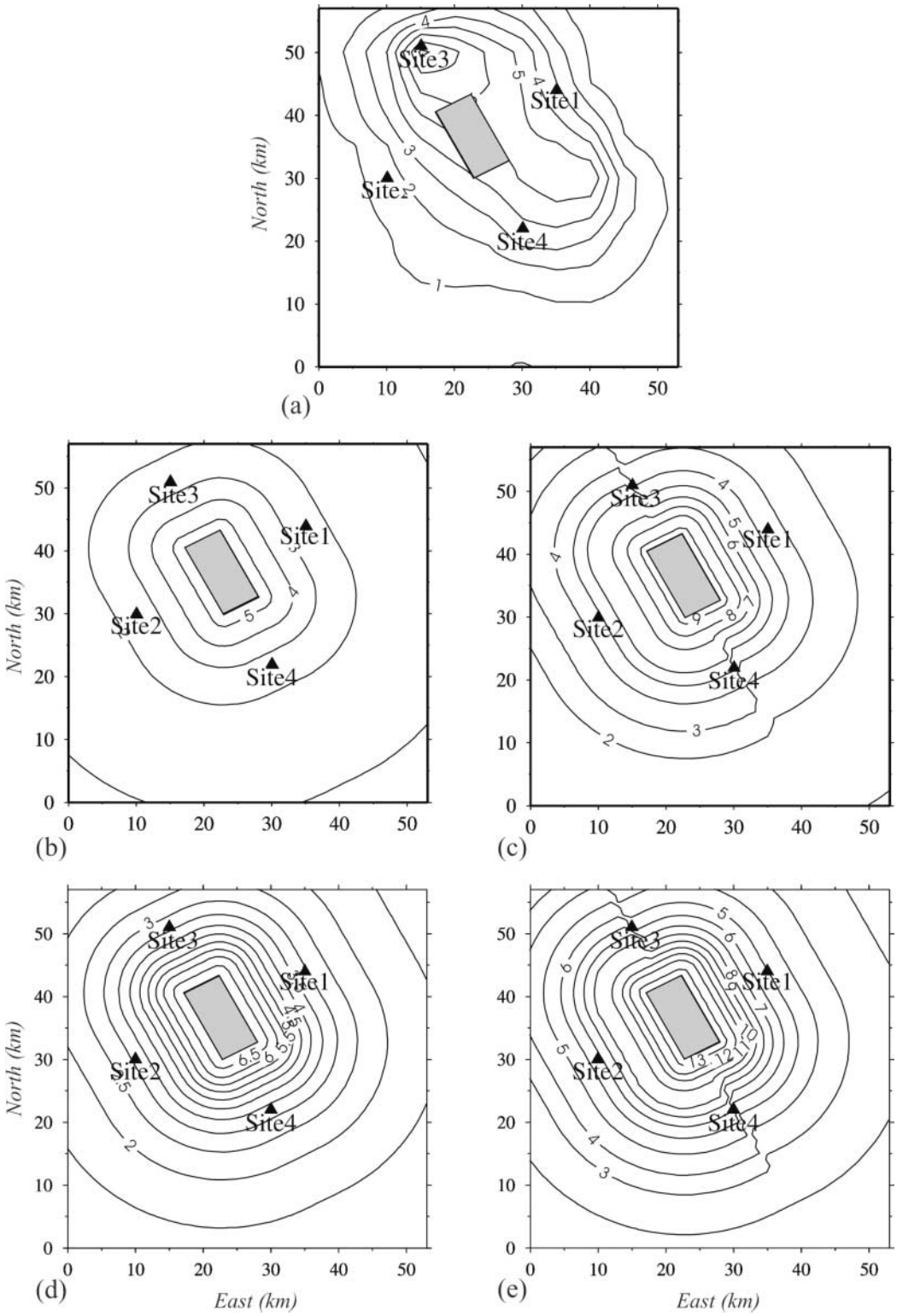

Figure 7. Same as Figure 5 but for $T_3 = 50{,}000$ years return period.

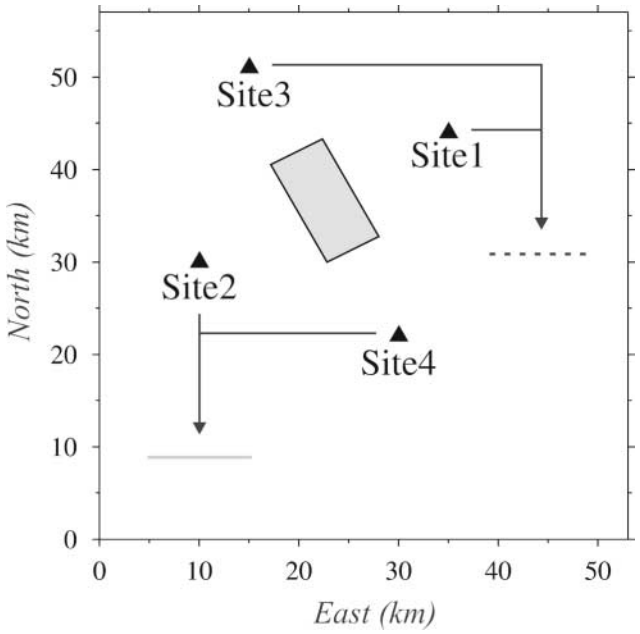

Figure 8. Site locations with respect to the surface fault projection (gray box) considered for the site-specific hazard analysis. Arrows refer to line style in Figures 9 and 10.

thetic data show PGA values lower than those obtained when the attenuation relationships are used to compute the earthquake effects. The site-specific hazard analyses also show differences in the shape of the hazard curves (Figs. 9 and 10), which is related, in particular, to the way that the earthquake effects and the associate uncertainties are estimated.

Acknowledgments

We thank the two anonymous reviewers and Associate Editor I. G. Wong for their thoughtful reviews and suggestions that greatly improved this manuscript. The figures were prepared with Generic Mapping Tools (Wessel and Smith, 1991). This work was financially supported by MIUR (PON-TECSAS), AMRA (Regione Campania–Center of Competence on Environmental Risks), and Italian Dipartimento della Protezione Civile (in the frame of 2004–2006 agreement with Istituto Nazionale di Geofisica e Vulcanologia).

References

Abrahamson, N. A., and W. J. Silva (1997). Empirical response spectral attenuation relations for shallow crustal earthquakes, *Seism. Res. Lett.* **68,** 94–127.

Aki, K. (1967). Scaling law of seismic spectrum, *J. Geophys. Res.* **72,** 1217–1231.

Aki, K., and P. G. Richards (1980). *Quantitative Seismology, Theory and Methods*, 2 Vols, W. H. Freeman, San Francisco, 932 pp.

Andrews, D. J. (1981). A stochastic fault model, 2, time-dependent case, *J. Geophys. Res.* **86,** 10,821–10,834.

Azimi, Sh. A., A. V. Kalinin, and B. L. Pivovarov (1968). Impulse and transient characteristics of media with linear and quadratic absorption laws, *Izv. Phys. Solid Earth* **2,** 88–93.

Boore, D. M., W. B. Joyner, and T. E. Fumal (1997). Equations for estimating horizontal response spectra and peak acceleration from Western North American earthquakes: a summary of recent work, *Seism. Res. Lett.* **68,** 128–153.

Camassi, R., and M. Stucchi (1996). NT4.1: un catalogo parametrico di terremoti di area italiana al di sopra della soglia del danno, CNR-GNDT, Milano, 1–86.

Capuano, P., A. Zollo, A. Emolo, S. Marcucci, and G. Milana (2000). Rupture mechanism and source parameter of Umbria-Marche main shocks from strong motion data, *J. Seism.* **4,** 436–478.

Cochard, A., and R. Madariaga (1996). Complexity of seismicity due to highly rate-dependent friction, *J. Geophys. Res.* **101,** 25,321–25,336.

Convertito, V., and A. Herrero (2004). Influence of focal mechanism in probabilistic seismic hazard analysis, *Bull. Seism. Soc. Am.* **94,** 2124–2136.

Cornell, C. A. (1968). Engineering seismic risk analysis, *Bull. Seism. Soc. Am.* **58,** 1583–1606.

Cornell, C. A., and E. H. Van Marke (1969). The major influences on seismic risk, in *Proc. Third World Conf. on Earthquake Engineering*, Santiago, Chile, A-1, 69–93.

Farra, V., P. Bernard, and R. Madariaga (1986). Fast near source evaluation of strong ground motion for complex source models, in *Earthquake Source Mechanics*, S. Das, J. Boatwright, and C. H. Scholz (Editors), American Geophysical Monograph **37,** 121–130.

Hanks, T. C. (1982). fmax, *Bull. Seism. Soc. Am.* **72,** 1867–1880.

Hanks, T. C., and H. Kanamori (1979). A moment magnitude scale, *J. Geophys. Res.* **84,** 2348–2350.

Heaton, T. H. (1990). Evidence for and implications of self-healing pulses of slip in earthquake rupture, *Phys. Earth Planet. Interiors* **64,** 1–20.

Herrero, A., and P. Bernard (1994). A kinematic self-similar rupture process for earthquakes, *Bull. Seism. Soc. Am.* **84,** 1216–1229.

Joyner, W. B., and D. M. Boore (1981). Peak horizontal acceleration and velocity from strong-motion records including records from the 1979 Imperial Valley, California earthquake, *Bull. Seism. Soc. Am.* **71,** 2011–2038.

Meghraoui, M., T. Camelbeeck, K. Vanneste, M. Brondell, and D. Jongmans (2000). Active faulting and paleoseismology along the Bree fault, lower Rhine graben, Belgium, *J. Geophys. Res.* **105,** 13,809–13,841.

Nielsen, S. B., L. Knopoff, and A. Tarantola (1995). Model of earthquake recurrence: role of elastic wave radiation, relaxation of friction, and inhomogeneity, *J. Geophys. Res.* **100,** 12,423–12,430.

Pantosti, D., and G. Valensise (1990). Faulting mechanism and complexity of the November 23, 1980, Campania-Lucania earthquake, inferred from surface observations, *J. Geophys. Res.* **95,** 15,319–15,341.

Pantosti, D., D. Schwartz, and G. Valensise (1993). Paleoseismicity along the 1980 surface rupture of the Irpinia fault: implications for earthquake recurrence in the Southern Apennines, Italy, *J. Geophys. Res.* **98,** 6561–6577.

Reiter, L. (1990). *Earthquake Hazard Analysis*, Columbia University Press, New York, 254 pp.

Rice, J. R. (1993). Spatio-temporal complexity of slip on fault, *J. Geophys. Res.* **98,** 9885–9907.

Sabetta, F., and A. Pugliese (1987). Attenuation of peak horizontal acceleration and velocity from Italian strong-motion records, *Bull. Seism. Soc. Am.* **77,** 1491–1513.

Schwartz, D. P., and J. Coppersmith (1984). Fault behaviour and characteristic earthquakes: examples from Wasatch and San Andreas faults, *J. Geophys. Res.* **89,** 5681–5698.

Somerville, P. G., H. F. Smith, R. W. Graves, and N. A. Abrahamson (1997). Modification of empirical strong ground motion attenuation relationship to include the amplitude and duration effects of rupture directivity, *Seism. Res. Lett.* **68,** no. 1, 199–222.

Tosi, P., A. Tertulliani, V. de Rubeis, and C. Gasparini (1999). Preliminary results of a macroseismic survey of the Colfiorito sequence (Central Italy). *Phys. Chem. Earth A* **24,** 477–181.

Valensise, G., R. Basili, M. Mucciarelli, and D. Pantosti (Editors) (2001). Database of potential sources for earthquakes larger than M 5.5 in Europe, a compilation of data collected by partners of EU project FAUST, www.ingv.it/~roma/banche/catalogo_europeo/index.html.

Wessel, P., and W. H. F. Smith (1991). Free software helps map and display data, *EOS Trans. AGU* **72,** 441, 445–446.

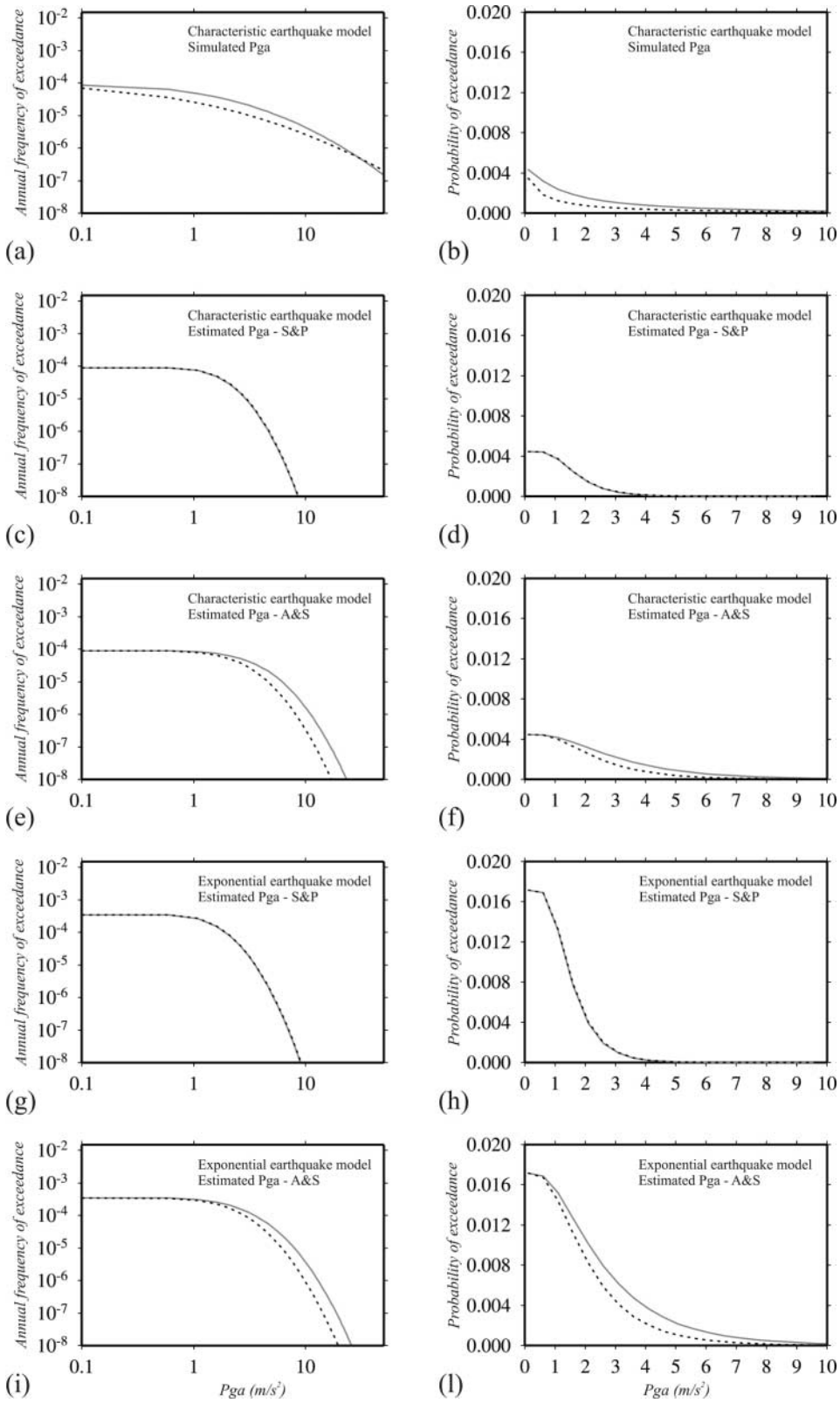

Figure 9. Hazard curves for the characteristic and the exponential recurrence models for sites 1 (dashed black lines) and 2 (gray lines). Annual frequency of exceedance is computed both by our technique (a) and by attenuation relationships. In particular, panels (c) and (g) refer to the characteristic and exponential models, respectively, when the Sabetta and Pugliese (1987) attenuation relationship (S&P) is used to estimate the PGA; panels (e) and (i) refer to the characteristic and exponential model, respectively, when the Abrahamson and Silva (1997) attenuation relationship (A&S) is used to estimate the PGA. The corresponding probability of exceedance curves for a 50-year exposure are also computed both by our technique (b) and by attenuation relationships (d, f, h, and l). Refer to Figure 8 for the site locations and the line style.

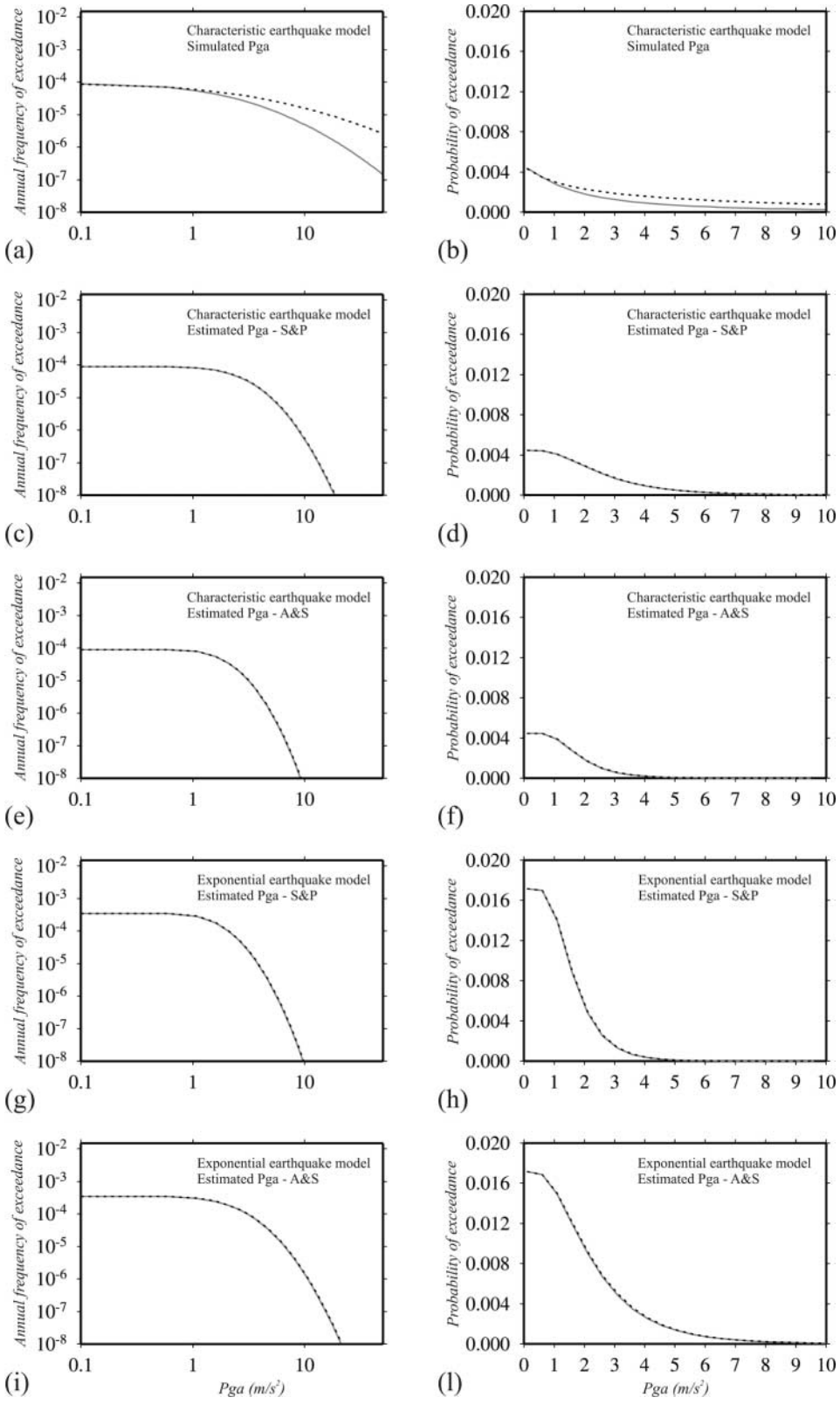

Figure 10. Same as Figure 9 but for the sites 3 and 4.

Youngs, R. R., and K. Coppersmith (1985). Implications of fault slip rates and earthquake recurrence models to probabilistic seismic hazard estimates, *Bull. Seism. Soc. Am.* **58,** 939–964.

Zollo, A., A. Bobbio, A. Emolo, A. Herrero, and G. De Natale (1997). Modeling of ground acceleration in the near source range: the case of 1976, Friuli earthquake (M = 6.5), Northern Italy, *J. Seism.* **1,** 305–319.

Zollo, A., S. Martucci, G. Milana, and P. Capuano (1999). The 1997 Umbria-Marche (Central Italy) earthquake sequence: insights on the main shock ruptures from near source strong motion records, *Geophys. Res. Lett.* **26,** 3165–3168.

Appendix

To simulate the ground acceleration at the Earth's surface radiated from an extended fault, we adopt a technique based on the far-field approximation of the wave field (Aki and Richards, 1980):

$$\partial^2 \vec{u}_c(\vec{r},t)/\partial t^2 = \frac{\partial}{\partial t^2} \int_{\Sigma}\int \vec{G}(\vec{r},\vec{r}_0,t) * \frac{\partial \Delta u(\vec{r}_0,t)}{\partial t}\, d\Sigma, \quad \text{(A1)}$$

where Δu is the slip function at the point $\vec{r}_0$ on the fault, and $\vec{G}$ is the Green's function for a point dislocation source and Σ is the fault surface.

Following Farra *et al.* (1986) the Green's function of a direct body wave in a layered elastic medium can be expressed as:

$$\vec{G}^{FF,c}(\vec{r},\vec{0},t) = \frac{\mu_0}{4\pi\rho_0 c_0^3} \mathrm{Re}\left\{\sqrt{\frac{\rho_0 c_0}{\rho c J}}\, \vec{F}_c \, \Pi \dot{\Delta}[t - T_c(\vec{r}_0)]\right\}, \quad \text{(A2)}$$

where μ and ρ are the rigidity and the density, respectively, and c is either the *P*- or *S*-wave velocity, according to the type of wave under consideration (the suffix 0 means "evaluated at the source"). The term J represents the geometric spreading factor, and $\vec{F}_c$ is a vector radiation pattern that depends on the takeoff angle of the ray at the source and on the geometric properties of the dislocation source. The quantity Π contains the product of all of the complex reflection and transmission coefficients at the different interfaces encountered by the ray on its trajectory. The function Δ is given by $\Delta(t) = \delta(t) - i/\pi t$, and T_c is the travel time. Each Green's function is convolved with the Azimi attenuation function (Azimi *et al.*, 1968) based on parameters defined by a constant quality factor Q_c to account for the Earth's anelasticity. The slip function in equation (A.1) is approximated by a ramp function:

$$\Delta u(\vec{r}_0,t) = \begin{cases} 0 & \text{for } t < T_R(\vec{r}_0) \\ \dfrac{D(\vec{r}_0)}{\tau(\vec{r}_0)}\,[t - T_R(\vec{r}_0)] & \text{for } T_R(\vec{r}_0) < t < T_R(\vec{r}_0) + \tau(\vec{r}_0), \\ D(\vec{r}_0) & \text{for } t > T_R(\vec{r}_0) + \tau(\vec{r}_0) \end{cases} \quad \text{(A3)}$$

where $D(\vec{r}_0)$, $\tau(\vec{r}_0)$, and $T_R(\vec{r}_0)$ represent the final slip, the rise time, and the rupture time associated with the fault element with a position of $\vec{r}_0$, respectively.

Under a constant rupture velocity hypothesis, the ω-square behavior of the seismic ground-motion spectra (Aki, 1967) can be related to self-similar slip and stress-drop distributions over the fault, which follow a negative power law as a function of the radial wave number k (Andrews, 1981; Hanks, 1982; Herrero and Bernard, 1994). We adopted the k-square model to obtain a heterogeneous final slip distribution on the fault plane from the two-dimensional inverse Fourier transform of the complex function:

$$\tilde{D}(k_x,k_y) = C \frac{1}{1 + \left(\dfrac{k}{k_c}\right)^2} e^{i\varphi(k_x,k_y)}, \quad \text{(A4)}$$

where $k = \sqrt{k_x^2 + k_y^2}$ is the radial wavenumber. The cutoff wavenumber, k_c, corresponds to the minimum fault dimension (e.g., Herrero and Bernard, 1994) and represents the characteristic dimension of the fault. When $k > k_c$, the dislocation is supposed to be incoherent on the fault plane, and in this case, the phase φ in equation (A4) is chosen randomly. The slip distribution is then tapered by a two-dimensional cosine-taper filter, to avoid unrealistically sharp slip transitions at fault edges. Finally, the constant C in equation (A4) is evaluated by normalizing the slip distribution, to obtain an *a priori* value of seismic moment. If a constant rupture velocity is used, the far-field seismic radiation is dominated by the slip heterogeneity instead of the irregularities in the rupture velocity distribution. This approximation may not be valid for highly discontinuous fracture phenomena, but it is reasonable when the rupture velocity varies smoothly along the fault.

The rise-time value in equation (A3) is generally chosen as the cutoff frequency of the low-pass filter that is applied to the synthetic seismograms. This corresponds to considering a deltalike slip velocity in equation (A1) and, in this case, the onset of slip appears to be instantaneous with the passage of the rupture front. In other words, it is assumed that the high-frequency seismic radiation is completely emitted next to the rupture front, in agreement with the observations by Heaton (1990). Because of the low-pass-filtering effect introduced on synthetics by a finite value of the rise time, this choice maximizes the expected amplitude of the ground motion in the far-field approximation.

The representation integral in equation (A1) is evaluated numerically by dividing the fault into discrete subfaults and then by summing their contributions. A fine fault grid is

needed to calculate the representation integral up to high frequencies, to avoid undesired numerical effects due to the fault dividing (e.g., spatial aliasing). Zollo *et al.* (1997) suggested characteristic subfault dimensions of about 20–30 m.

Dipartimento di Scienze Fisiche
Università degli Studi "Federico II" di Napoli
80124 Napoli, Italy